Supplement of Atmos. Chem. Phys., 16, 12601–12629, 2016
http://www.atmos-chem-phys.net/16/12601/2016/
doi:10.5194/acp-16-12601-2016-supplement

Atmospheric Chemistry and Physics Open Access EGU

Supplement of

Vertical profiles of aerosol and black carbon in the Arctic: a seasonal phenomenology along 2 years (2011–2012) of field campaigns

Luca Ferrero et al.

Correspondence to: Luca Ferrero (luca.ferrero@unimib.it

Conc (ng m^{-3})	HO		PG		NG		DNG		Detection Limit
	mean	σ_m	mean	σ_m	mean	σ_m	mean	σ_m	
Na^+	410.85	252.44	655.24	293.67	590.94	192.18	325.71	84.23	0.04
NH_4^+	66.33	13.85	74.61	12.22	85.04	15.89	128.31	29.21	0.4
K^+	21.73	8.43	28.81	9.50	27.34	5.98	23.94	2.40	0.04
Mg^{2+}	54.21	27.28	79.34	31.70	73.35	20.50	51.21	13.16	0.04
Ca^{2+}	39.45	7.67	43.28	7.07	38.88	4.71	33.45	3.17	0.04
Cl^-	495.82	332.03	871.20	392.54	745.67	267.28	357.20	173.05	0.04
NO_2^-	22.51	10.00	36.00	15.66	31.43	11.98	20.06	2.33	0.04
NO_3^-	59.92	12.96	68.66	12.22	51.64	9.59	49.37	15.90	0.04
SO_4^{2-}	504.71	93.15	584.69	72.69	779.09	204.18	1441.91	354.09	0.04
Oxalates	4.79	0.98	5.46	0.54	4.99	0.50	6.97	1.12	0.4
F^-	0.18	0.08	0.21	0.13	0.07	0.09	<DL	<DL	0.004
Glycolate	1.16	0.16	1.29	0.29	1.05	0.14	1.27	0.19	0.4
Formate	2.15	0.70	2.92	0.68	2.99	0.47	2.78	0.38	0.4
MSA	2.28	0.58	4.47	1.07	3.57	0.81	1.84	0.36	0.04
EC	<DL	<DL	<DL	<DL	<DL	<DL	31.85	0.20	11
OC	534.36	39.52	522.87	52.69	517.13	43.96	689.94	19.59	120

Table S1. Ambient concentrations (ng m^{-3}) of the aerosol chemical components (mean±mean standard deviation) and their analytical detection limits (DL). Data are reported for the springtime samples collected at ground during: a) homogeneous profiles (HO); b) positive gradient profiles (PG); c) negative gradient profiles (NG); d) decoupled negative gradient profiles (DNG).

Intrument size		Ambient size (μm)	
OPC Channel	PSL (μm)	Spring	Summer
1	0.25	0.26	0.26
2	0.28	0.29	0.29
3	0.30	0.31	0.31
4	0.35	0.37	0.37
5	0.40	0.43	0.43
6	0.45	0.49	0.50
7	0.50	0.53	0.54
8	0.58	0.69	0.71
9	0.65	0.73	0.75
10	0.70	0.77	0.79
11	0.80	0.93	0.94
12	1.00	1.20	1.24
13	1.30	2.24	2.37
14	1.60	2.48	2.54
15	2.00	2.66	2.72
16	2.50	3.89	4.17
17	3.00	4.79	5.25
18	3.50	6.61	7.16
19	4.00	7.67	8.41
20	5.00	9.77	10.47
21	6.50	16.03	16.60
22	7.50	17.58	18.20
23	8.50	19.72	20.18
24	10.00	23.99	24.55
25	12.50	30.20	30.55
26	15.00	35.89	36.31
27	17.50	41.69	42.17
28	>20.00	>47.32	>47.86

Table S2. Original size channels of OPC Grimm 1.107 calibrated with PSL spheres (left side) and corrected (right side, columnar average) for the ambient refractive index for spring and summer.

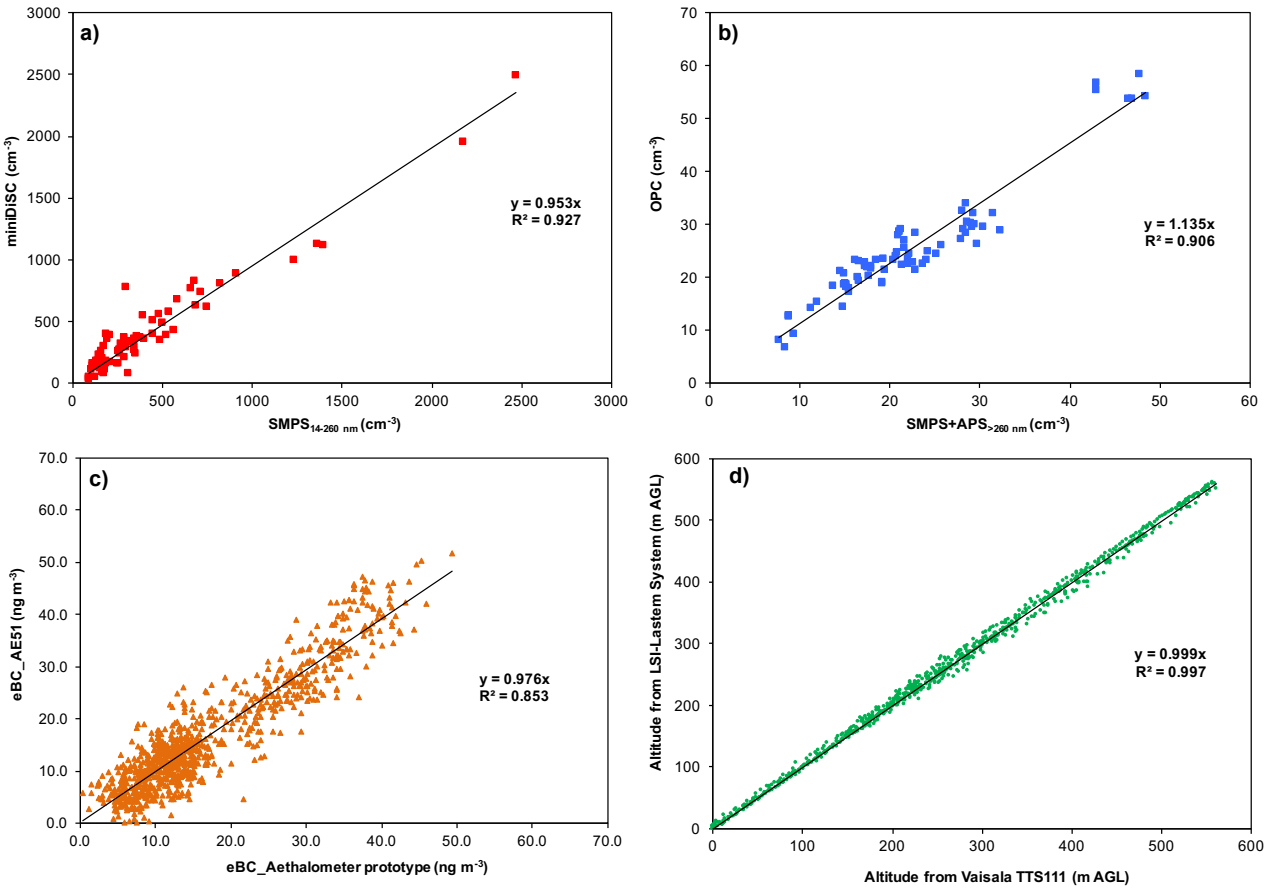

Figure S1. Linear correlations between: a) $N_{14\text{-}260}$ measured with the miniDiSC and with the SMPS; b) $N_{>260}$ measured with the OPC and with the SMPS+APS; c) eBC measured with AE51 and the micro-Atehalometer prototype; d) altitude obtained with the LSI-Lastem meteorological station and with the Vaisala tethersonde.

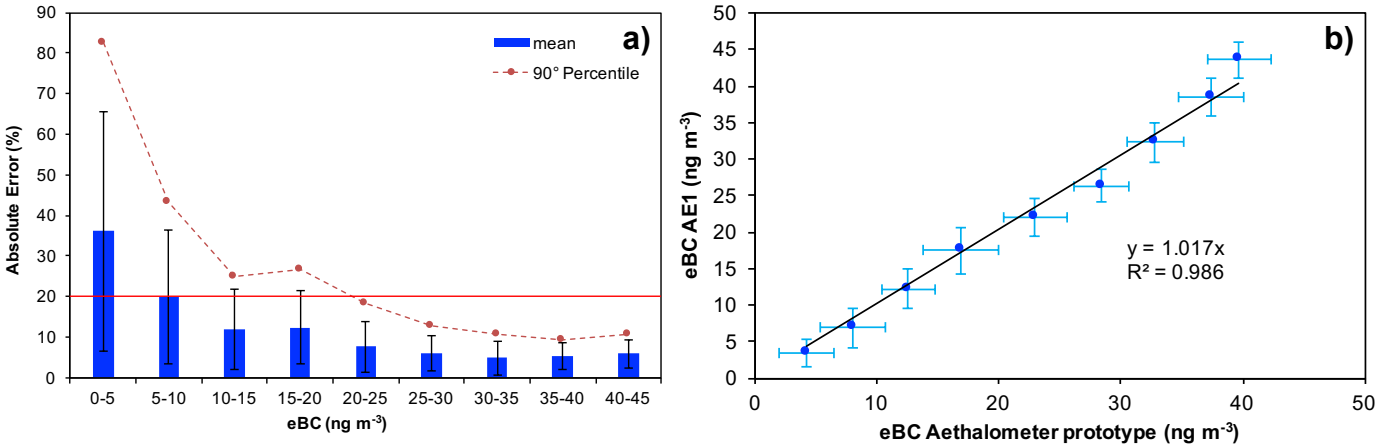

Figure S2. a) Absolute value of the error in percentage of the measured eBC in function of its concentration (5 ng m^{-3} intervals); b) correlation between the eBC concentrations (AE51 and prototype) averaged on 5 ng m^{-3} intervals.

Effect of absorbing and non-absorbing particles on eBC measurements

It should be noted that absorbing non-BC particles may contribute to the signal in Aethalometers (i.e. Brown Carbon, dust). However, BrC is characterized by negligible absorption in the infrared (Andreae and Gelencsér, 2006), the wavelength range of the eBC measurements (micro-Aeth AE51 uses 880 nm). In this respect, Massabò et al. (2013) showed the potential contribution of BrC to the determination of eBC to be below 10%.

To estimate the possible influence of BrC on eBC measurements carried out during the spring 2011 campaign, the data collected with the micro-Aeth prototype at 370 and 880 nm were considered. Particularly, the Aethalometer model (Sandradewi et al., 2008) was applied to the apportionment of absorption due to both BC and BrC as reported in Massabò et al (2013) and in Shamjad et al. (2015) as follows:

$$\frac{b_{abs}(370\,nm)_{BC}}{b_{abs}(880\,nm)_{BC}} = \left(\frac{370}{880}\right)^{-\alpha_{BC}} \quad \text{(s1)}$$

$$\frac{b_{abs}(370\,nm)_{BrC}}{b_{abs}(880\,nm)_{BrC}} = \left(\frac{370}{880}\right)^{-\alpha_{BrC}} \quad \text{(s2)}$$

$$b_{abs}(\lambda) = b_{abs}(\lambda)_{BC} + b_{abs}(\lambda)_{BrC} \quad \text{(s3)}$$

where α_{BC} and α_{BrC} represent the Absoprtion Angstrom Exponents of BC and BrC, respectively. α_{BC} was 1 as suggested by Massabò et al (2013) and Sandradewi et al. (2008), while α_{BrC} was set at 3.5 (Yang et al., 2009), 3.95 (Massabò et al., 2013), 6.6 (Shamjad et al., 2015) and 9.0 (Bikkina et al., 2013), respectively. With this inputs, the percentage of absorption coefficient at 880 nm due to BrC instead that BC was 8.5%, 5.8%, 0.5% and 0.1%, respectively. Thus, it is possible to estimate that the BrC positive artifact on eBC measurements was less than 10% during the campaign.

For what concern the non-absorbing particles, they can affect the attenuation by enhancing the backscattering of the filter plus aerosol system. In this respect, during the campaign the experimental protocol followed that reported in Ferrero et al. (2011). All vertical BC profiles were conducted by changing the filter ticket regularly. As a result, ATN never achieved values higher than 20 during all profiles. This means that the total amount of aerosol collected on each filter during the vertical profile was very low making the effect of non-absorbing particles negligible.

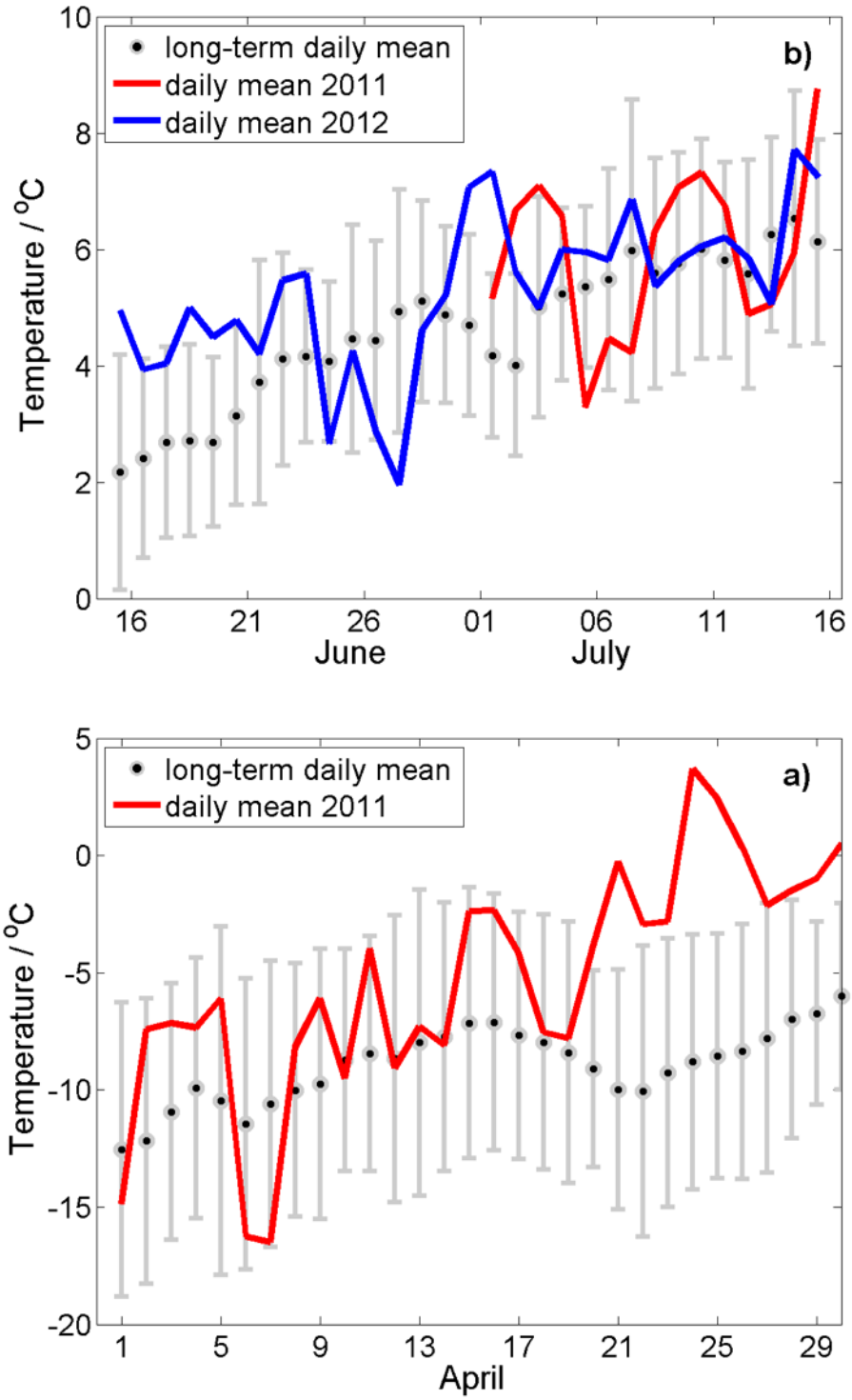

Figure S3. Daily mean temperature during the campaign periods (a) spring 2011, (b) summer 2011 and summer 2012, in comparison to the 20-year longterm daily mean (1993-2015, excluding 2011 and 2012).

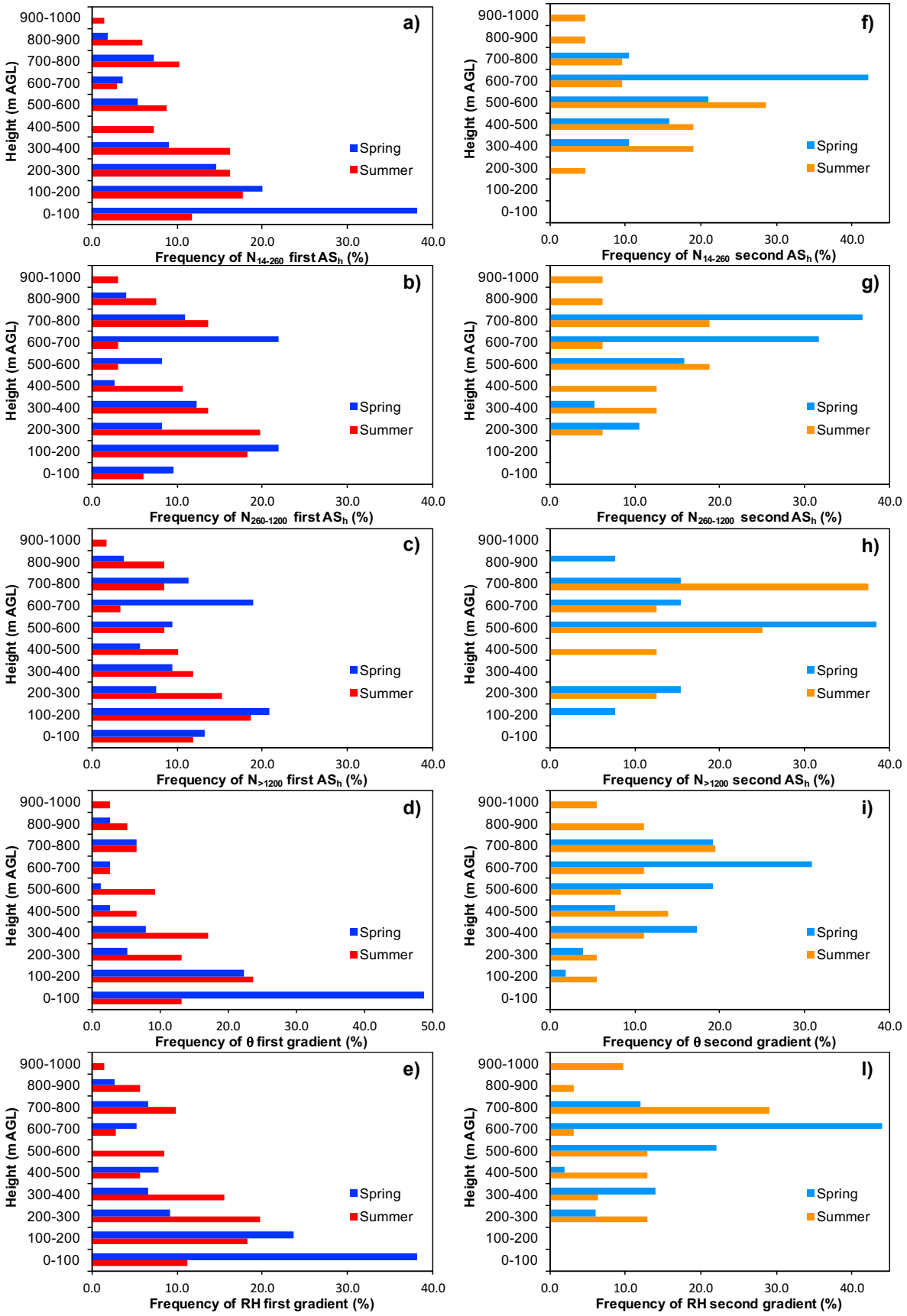

Figure S4. Vertical frequency distribution of the first and second AS_h for $N_{14\text{-}260}$, $N_{260\text{-}1200}$, $N_{>1200}$, θ and RH during spring and summer.

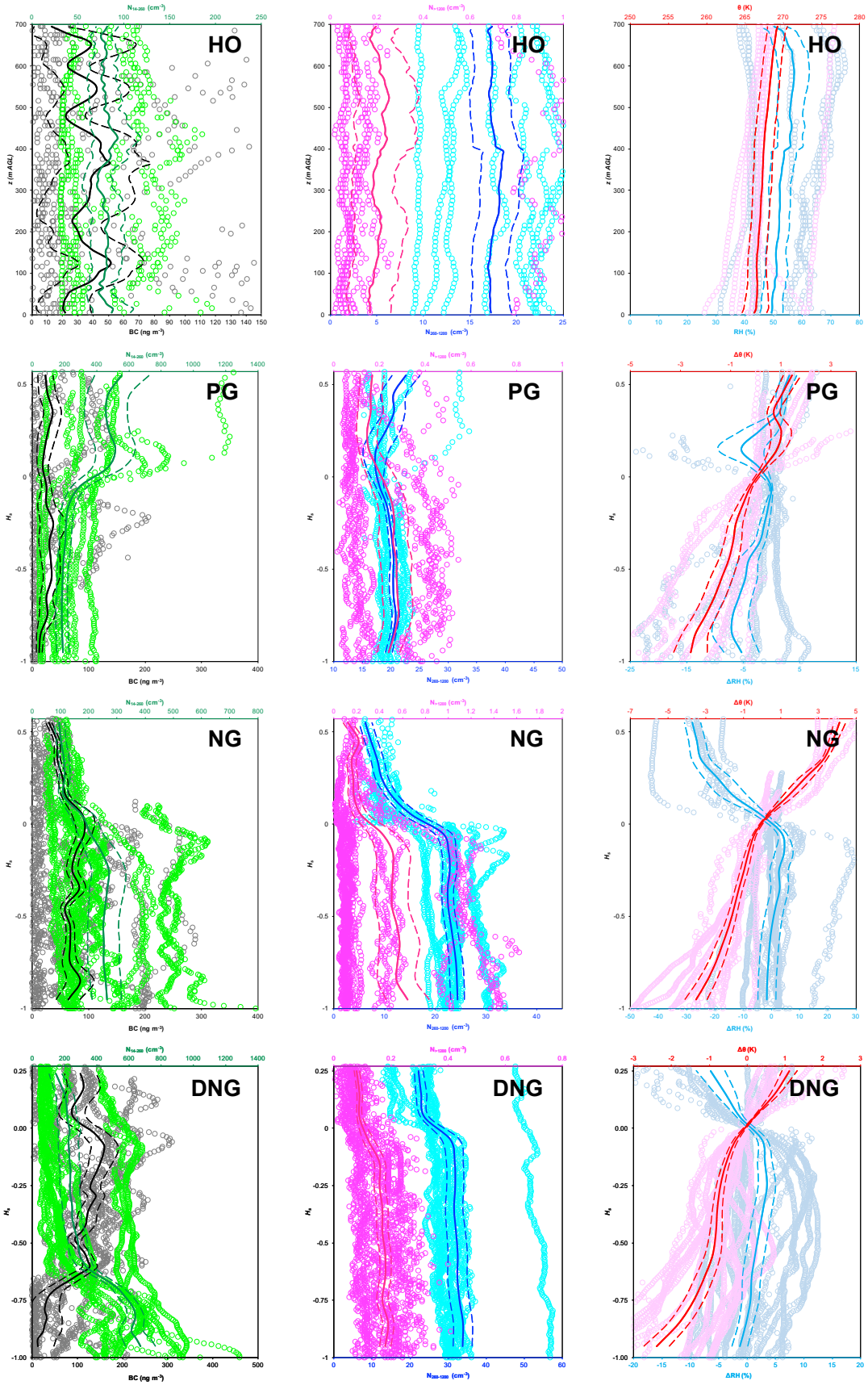

Figure S5. All data point of the collected vertical profiles during spring for each profile class. The average (solid line) and the mean standard deviation (dashed lines) are also reported.

Origin of air masses and vertical profile typology

Air mass origin is important when studying the Arctic aerosol. However, before trying to find a relationship between the shape of the vertical profile and air mass origin, it is necessary to consider that each profile shape is the result of an interplay among several processes: 1) transport events, 2) the planetary boundary layer dynamic and 3) the local formation of aerosol.

Among this, only the transport event process is strongly related to the air mass origin (some precursors transported may also affect secondary aerosol formation), while the final profile shape is the result of the specific combination of the aforementioned processes.

Figure 7 in the manuscript represents a good example in which the same air mass originated two different typology of profiles. Particularly, the transported polluted air masses from mid-latitudes generated initially PG profiles that naturally evolved (due to the entrance into the PBL) into NG profiles.

Thus, the same air mass origin could be related to different profile classes.

Back-trajectories corresponding to each profile class were calculated carried out using the Hysplit 4 (rev. 513) model feeded by NCEP GDAS 1x1 degree meteorological data. The calculated back-trajectories were propagated for 168 hours (7 days). The calculated back-trajectories reached the sampling site at 900, 1100, 1300 and 1500 m a.g.l.. A cluster analysis was performed on all the computed trajectories. For each group all the clusters fulfilling the criterion of a minimum 30% percent change in total spacial variance were calculated and the representing trajectories evaluated and compared. The result is reported in Figure S6.

From Figure S6 it is possible to observe first that back-trajectories were close in the Arctic area during HO profiles. HO profiles are then representative for background conditions in the Arctic. Both PG and NG can be affected by transport from mid-latitudes. The same happened for DNG profiles, which are a special type of NG profiles.

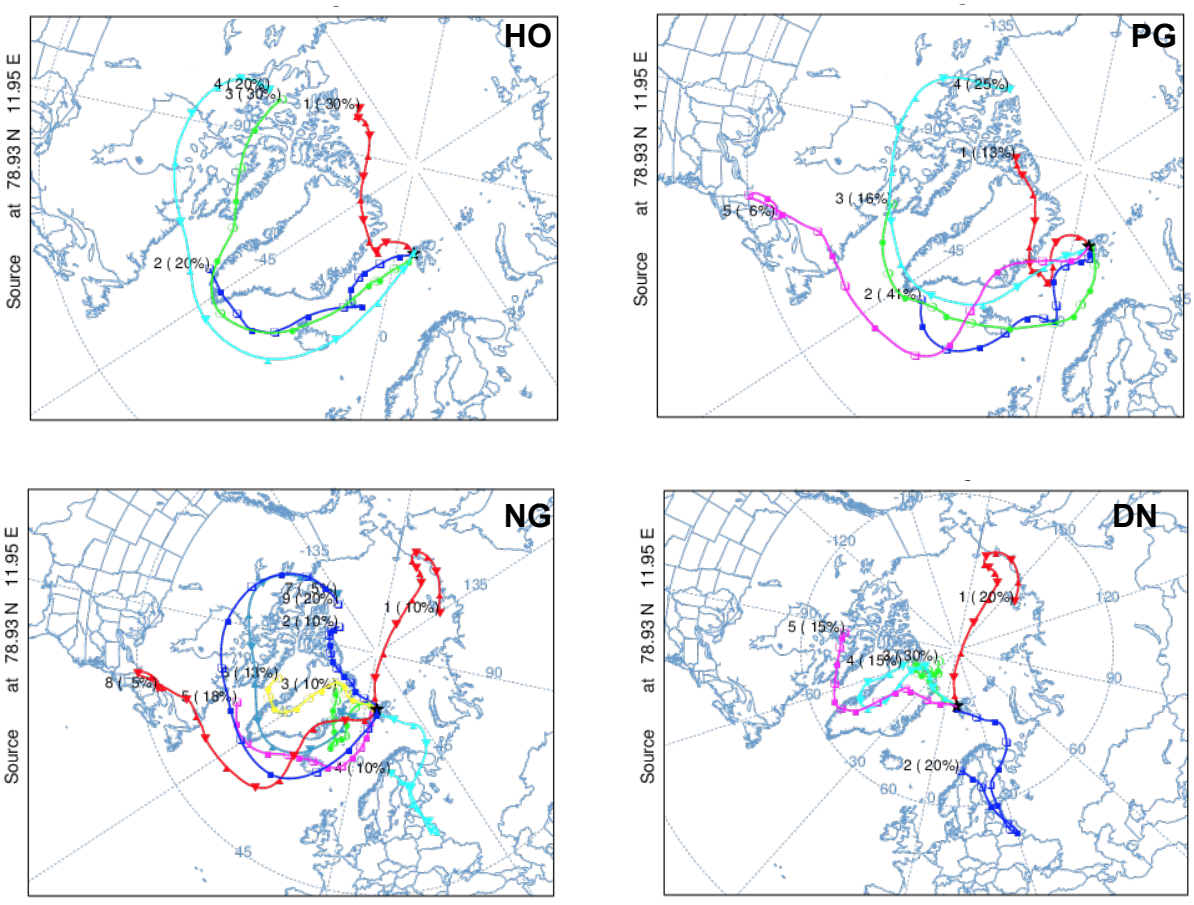

Figure S6. Cluster analysis of springtime back-trajectories for each profile class.

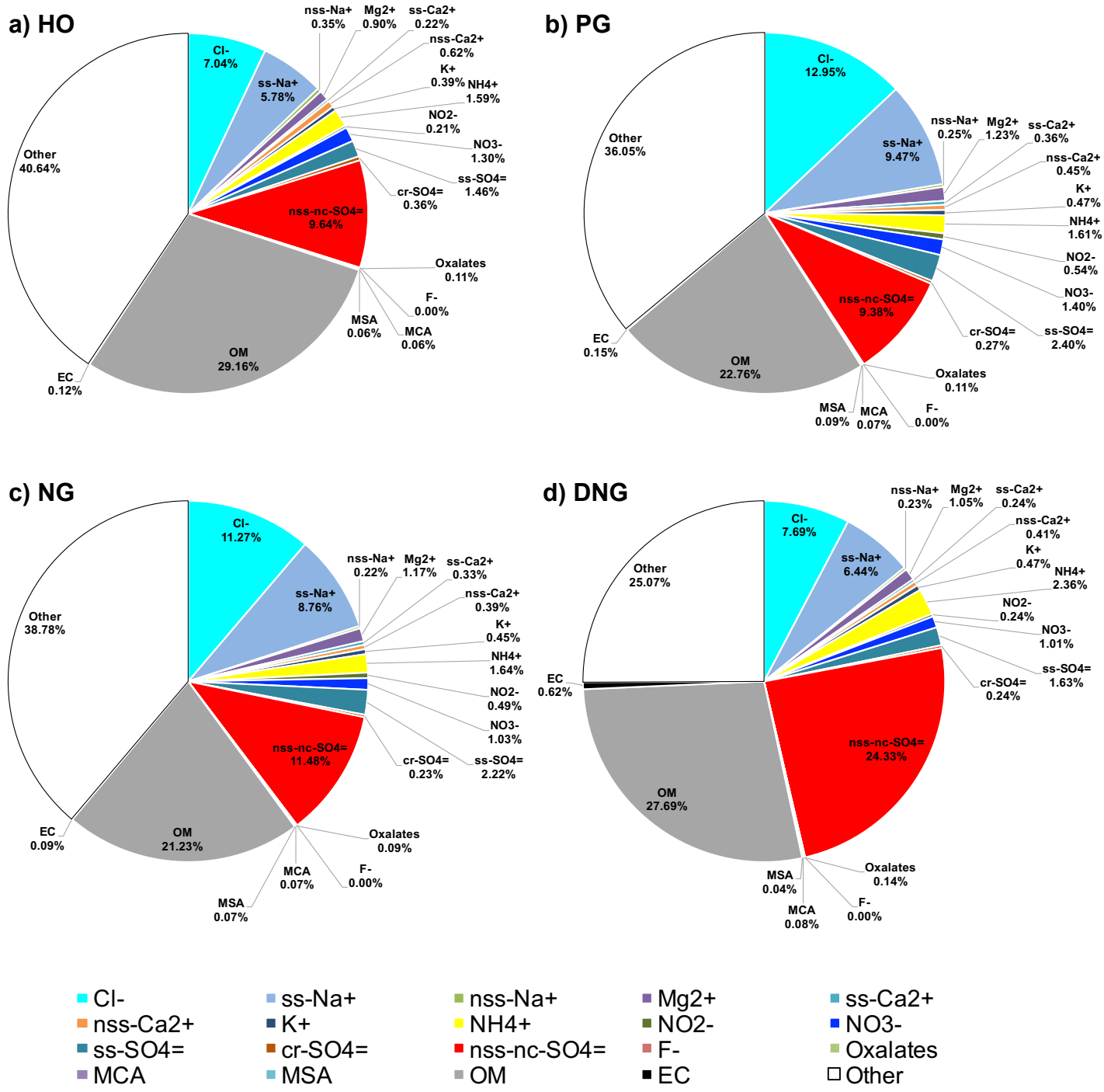

Figure S7. Springtime aerosol chemical composition determined at ground during: a) homogeneous profiles (HO); b) positive gradient profiles (PG); c) negative gradient profiles (NG); d) decoupled negative gradient profiles (DNG). Data shown are the respective aerosol mass fractions of each individual aerosol species.

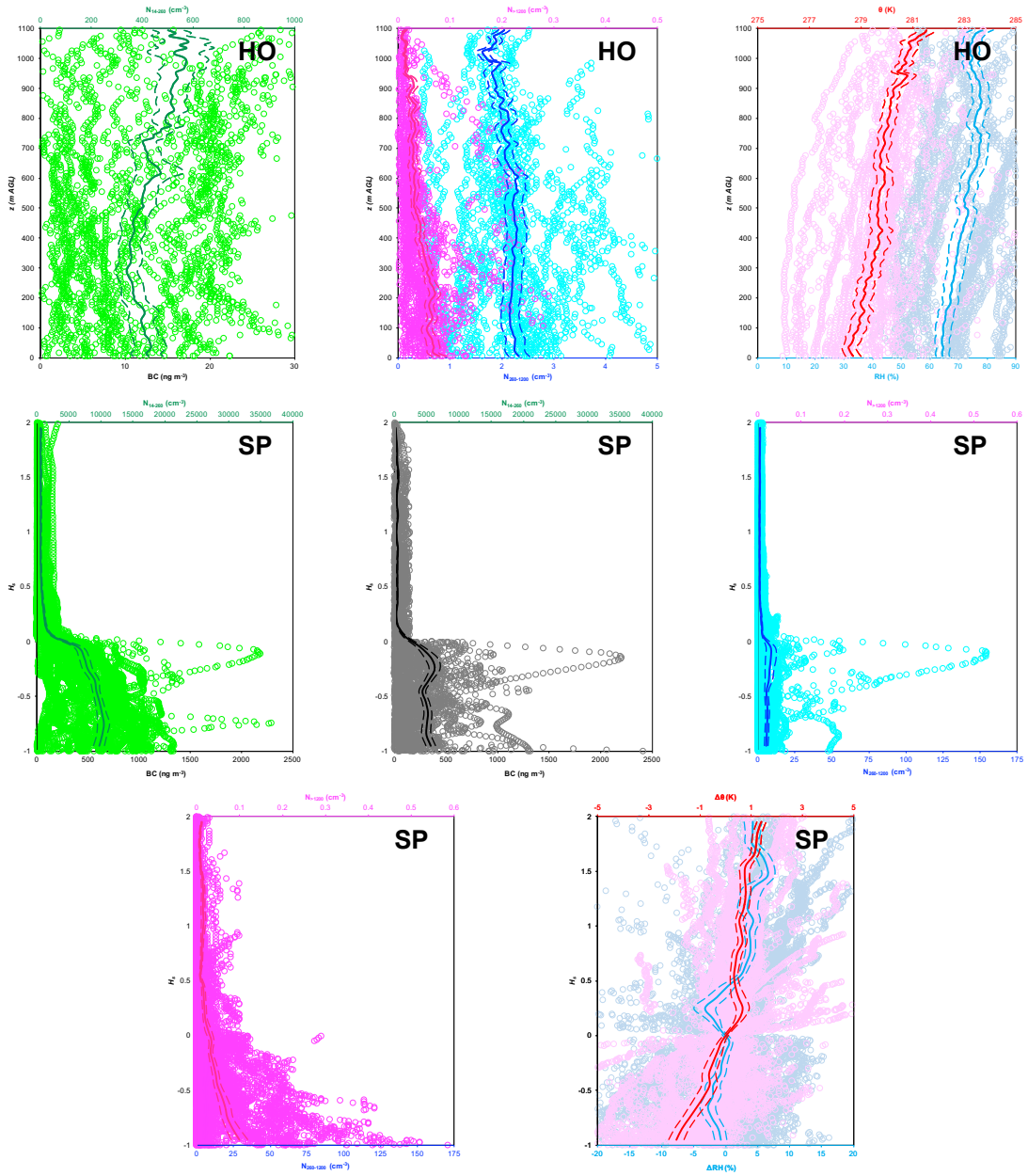

Figure S8. All data point of the collected vertical profiles during spring for each profile class. The average (solid line) and the mean standard deviation (dashed lines) are also reported.

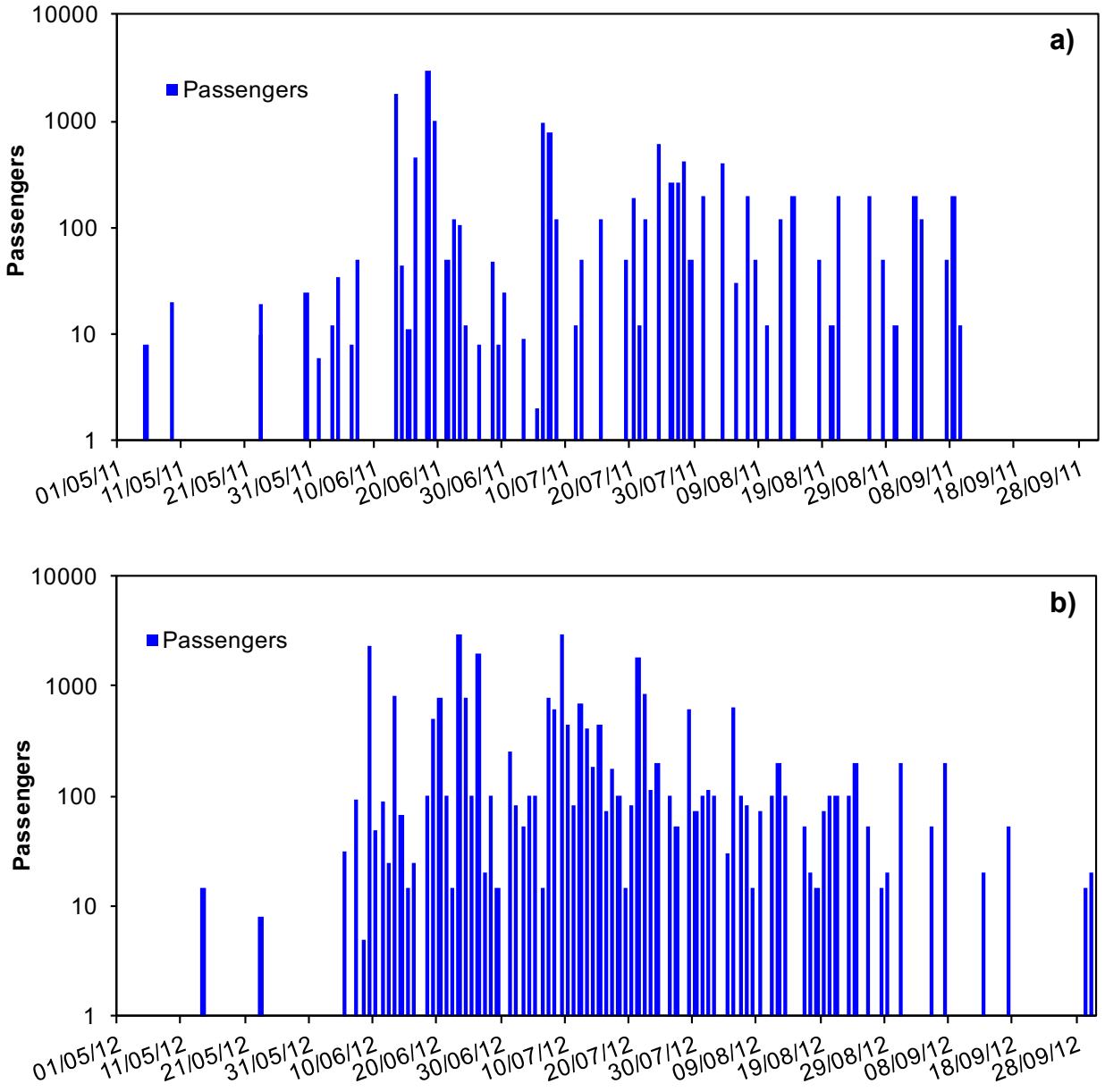

Figure S9. Dates and number of passengers registered by the Kings-Bay Kull Company for ships arrivals in Ny-Ålesund for: a) summer 2011 and b) summer 2012, respectively.

References

Andreae, M.O and Gelencsér A.: Black carbon or brown carbon? The nature of light-absorbing carbonaceous aerosols, Atmos. Chem. Phys., 6, 3131–3148, 2006.

Bikkina, S., Sarin, M.M.: Light absorbing organic aerosols (brown carbon) over the tropical Indian Ocean: impact of biomass burning emissions, Environ. Res. Lett., 8 (4), 044042, 2013.

Ferrero, L., Mocnik, G., Ferrini, B. S., Perrone, M. G., Sangiorgi, G. and Bolzacchini, E.: Vertical profiles of aerosol absorption coefficient from micro-Aethalometer data and Mie calculation over Milan., Sci. Total Environ., 409(14), 2824–37, doi:10.1016/j.scitotenv.2011.04.022, 2011.

Massabò, D., Caponi, L., Bernardoni, V., Bove, M.C., Brotto, P., Calzolai,, G., Cassola, F., Chiari, M., Fedi, M.E., Fermo, P., Giannoni, M., Lucarelli, F., Nava, S., Piazzalunga, A., Valli, G., Vecchi, R., Prati, P.: Multi-wavelength optical determination of black and brown carbon in atmospheric aerosols, Atmos. Environ., 108, 1-12, 2015.

Sandradewi, J., Prevot, A.H., Szidat, S., Perron, N., Rami Alfarra, M., Lanz, V., Weingartner, E., Baltensperger, U.: Using aerosol light absorption measurements for the quantitative determination of Wood burning and traffic emission contributions to particulate matter, Environ. Sci. Technol. 42, 3316-3323, 2008.

Shamjad, P.M., Tripathi, S.N., Pathak, R., Hallquist, M., Arola, A., and Bergin M.H.: Contribution of Brown Carbon to Direct Radiative Forcing over the Indo-Gangetic Plain, Environ. Sci. Technol., 49, 10474−10481, 2015.

Yang, M., Howell, S.G., Zhuang, J., Huebert, B.J.: Attribution of aerosol light absorption to black carbon, brown carbon, and dust in China e interpretations of atmospheric measurements during EAST-AIRE. Atmos. Chem. Phys. 9, 2035-2050, 2009.